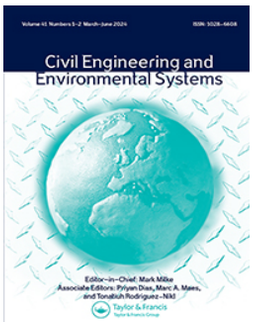

Civil Engineering and Environmental Systems

ISSN: (Print) (Online) Journal homepage: www.tandfonline.com/journals/gcee20

Accuracy of stochastic finite element analyses for the safety assessment of unreinforced masonry shear walls

Lewis J. Gooch, Mark G. Stewart & Mark J. Masia

To cite this article: Lewis J. Gooch, Mark G. Stewart & Mark J. Masia (10 Sep 2024): Accuracy of stochastic finite element analyses for the safety assessment of unreinforced masonry shear walls, Civil Engineering and Environmental Systems, DOI: 10.1080/10286608.2024.2400960

To link to this article: https://doi.org/10.1080/10286608.2024.2400960

Published online: 10 Sep 2024.

CIVIL ENGINEERING AND ENVIRONMENTAL SYSTEMS
https://doi.org/10.1080/10286608.2024.2400960

Accuracy of stochastic finite element analyses for the safety assessment of unreinforced masonry shear walls

Lewis J. Gooch[a,b], Mark G. Stewart[b] and Mark J. Masia[a]

[a]Centre for Infrastructure Performance and Reliability, The University of Newcastle, Callaghan, Australia;
[b]Centre for Built Infrastructure Resilience, University of Technology Sydney, Ultimo, Australia

ABSTRACT

To examine structural safety and reliability, an accurate prediction of the variability of structural resistance must first be determined. This may be achieved through extensive physical testing or, more commonly in modern research, synthetic data generation, such as stochastic finite element analyses (SFEAs). Due to the prevalence and versatility of such techniques, and the need for a high level of confidence when performing a safety assessment, an understanding of the accuracy of data derived from SFEAs is essential. In this paper, SFEA models have been developed to predict the responses of 16 unreinforced masonry walls tested in a laboratory under cyclic in-plane lateral loading. Each SFEA has been developed to reflect the as-built conditions of these experimental specimens and focus on predicting the shear capacity of the failure mechanisms that unreinforced masonry shear walls are susceptible to. From the results of these SFEAs, the accuracy (quantified as model error) of this modelling strategy has been estimated by comparing the peak in-plane shear resistances of the laboratory and numerical models.

KEYWORDS

Unreinforced masonry; shear walls; stochastic finite element analysis; spatial variability; model accuracy

1. Introduction

The reliability of a structure or structural element is defined by a relationship between a load effect and a corresponding structural resistance. In general, a structure will typically be considered to have failed if its resistance is exceeded by a destabilising load effect (Melchers and Beck 2018). Therefore, the accurate prediction of a structure's response is an essential component of examining structural safety and risk. A versatile tool for such predictions is that of numerical modelling, such as the finite element method (FEM). The utilisation of this tool allows for the structural response (load capacity, stiffness, ductility, etc.) to be examined for any configuration of a structural element without the need for expensive and time-intensive full-scale physical testing. Recent investigations of the variability and reliability of structural elements incorporate the FEM in the form of a stochastic finite element analysis (SFEA), such as the studies on out-of-plane loading of masonry walls by Isfeld, Stewart, and Masia (2021; 2023) and Muhit (2021).

CONTACT Lewis J. Gooch lewis.gooch@newcastle.edu.au

Due to both the versatility and prevalence of the FEM, the quantification of the accuracy of SFEA predictions of structural resistance is essential to structural reliability. As noted by Melchers (2007), errors associated with the adopted models of structural and material behaviours are prominent among the technical sources of structural failures. This is particularly relevant to reliability-based assessments where accuracy in the extreme cases of a structure's load carrying capacity (i.e. the configurations of material properties, structural dimensions and any stabilising load effects corresponding to a structure's most vulnerable state) can have a significant impact on predictions of safety.

There have been developments in the field of the structural reliability of load-bearing, masonry structures for the past 50 years (Ellingwood et al. 1980; Hart et al. 1983; Heffler et al. 2008; Mojsilović and Stewart 2015; Stewart and Lawrence 2007). However, the risk associated with unreinforced masonry (URM) walls subject to unfavourable stress states, such as the combined shear-tensile stresses induced under seismic or wind loading conditions, remains unquantified. This research gap is highly significant to the safety-in-design of structural masonry systems and the assessment and maintenance of the large number of existing URM structures. As wall elements are responsible, not only for the transfer of transient lateral loads into a structure's foundation but also of permanent and imposed gravity loading (and also the support of non-structural systems), a lack of understanding regarding the structural reliability of these systems equates to a lack of confidence in the safety of all load-bearing URM structures.

The vulnerability of URM walls subject to these highly variable loading conditions necessitates the accurate prediction of URM shear wall behaviour when designing new, or assessing existing, masonry structures. To examine the accuracy of contemporary methods of predicting the ultimate capacity of URM shear walls, seven spatially variable, SFEA models have been developed based on the laboratory testing performed in a previous study (Gooch et al. 2024). These numerical models have been developed using the simplified micro-modelling method, adapted from Lourenço (1996b), using the commercial finite element software package DIANA 10.3 (2019). This modelling methodology is common in masonry research (Howlader et al. 2020; Isfeld et al. 2021; Lourenço 2008) and allows for the nonlinear behaviour of the unit–mortar interface to be included while reducing the computational expense of each simulation. These attributes favour a spatially variable SFEA that requires both a large number of realisations, as well as a detailed material model of the critical failure surfaces.

The results of these SFEAs, in conjunction with the experimentally observed responses, allow for an investigation into the accuracy, presented as model error (ME), associated with this common modelling technique to be performed. Furthermore, a direct comparison between the SFEA predictions and the repeat laboratory tests allows for the limitations of this modelling methodology to be assessed, particularly with reference to the accuracy of capturing the load–displacement behaviour of specific URM shear wall failure mechanisms. These results can be used to inform the application of numerical methods of predicting URM behaviour, as well as facilitating the use of a correction for ME in applications such as a reliability analysis.

The SFEA method was adopted in the current study due both to its capacity to consider the spatial variability of material properties that is observed in masonry structures (Corrêa et al. 2012). Furthermore, to assess the reliability of a structural system, the variability of the system's capacity to resist destabilising load effects (commonly as a probability

density function (PDF)) must be determined (Melchers and Beck 2018). An approximation of this PDF cannot readily be made from conventional FEM, as all parameters utilised in this technique are deterministic and so, therefore, is the predicted structural resistance.

2. Configuration of wall models

The numerical models developed in this study are based upon the experimental specimens tested by Gooch et al. (2024). These experimental specimens were separated into four sets, each of which were designed to undergo a distinct failure mechanism of URM shear walls: namely (Set 1) flexural tension, (Set 2) flexural compression, (Set 3) shear sliding and (Set 4) diagonal tension. This numbering notation has been utilised in the subsequent sections to refer to these distinct experimental sets. Furthermore, all four specimens in a given experimental set were constructed by the same mason; Sets 1 and 2 were constructed by mason A, while Sets 3 and 4 were constructed by mason B (Gooch et al. 2024). The use of a different mason results in different qualities of workmanship for the distinct sets, a factor that is evident in the material characteristics presented in Section 2.3.

The geometry and load configurations of each SFEA are reflective of those adopted for the laboratory specimens. However, as discussed in Section 2.3, the material testing performed on the masonry utilised in the full-scale laboratory testing indicates that specimens cannot be readily divided based solely upon their distinctive geometries and boundary conditions. As such, the following sections outline the structural configurations of each SFEA, as well as the material models adopted for each analysis.

2.1. Geometry and boundary conditions

The wall specimens were modelled using the simplified micro-modelling method (Lourenço 1996b). These models used a single wythe of masonry units (110 mm wall thickness) and were 1194 mm tall (equivalent to a half-storey in height). Furthermore, SFEAs representing experimental Sets 1 and 2 were 1190 mm in length (aspect ratio equal to 1.0), while the models for Sets 3 and 4 were 1910mm in length (aspect ratio of 0.625) (refer to Figures 1a and b, respectively).

Each SFEA utilised boundary conditions consistent with the laboratory conditions. Vertical pre-compression was applied over a length of 240 mm at the top of the loading beam. The base of the concrete footing beam was restrained in both the horizontal and vertical directions. The tops of the truss elements shown in Figure 1(b) are supported via horizontal and vertical restraints representative of the pins supporting these elements in the laboratory set-up. In the case of the SFEA representing experimental Set 4, the shear stop applied at the bottom course of units has been modelled using a horizontal restraint applied to both ends of the modelled wall.

2.2. Loading scheme

The self-weight of the walls and the applied vertical pre-compression (F_y) was initially applied to each model. This loading was held constant during each SFEA. Prescribed lateral displacements (d_x) were then applied to the centre of the loading beam. Both monotonic and cyclic loading schemes were examined in the SFEAs (refer to Figure 2).

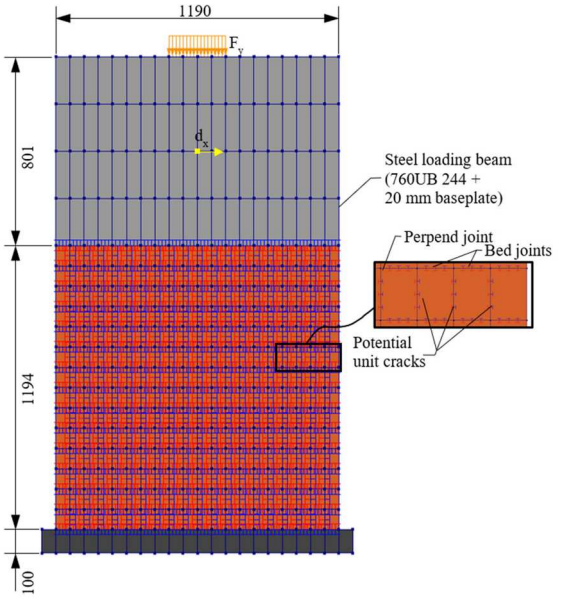

(a) Numerical models of experimental Sets 1 and 2 (cantilevered), and interface element breakdown.

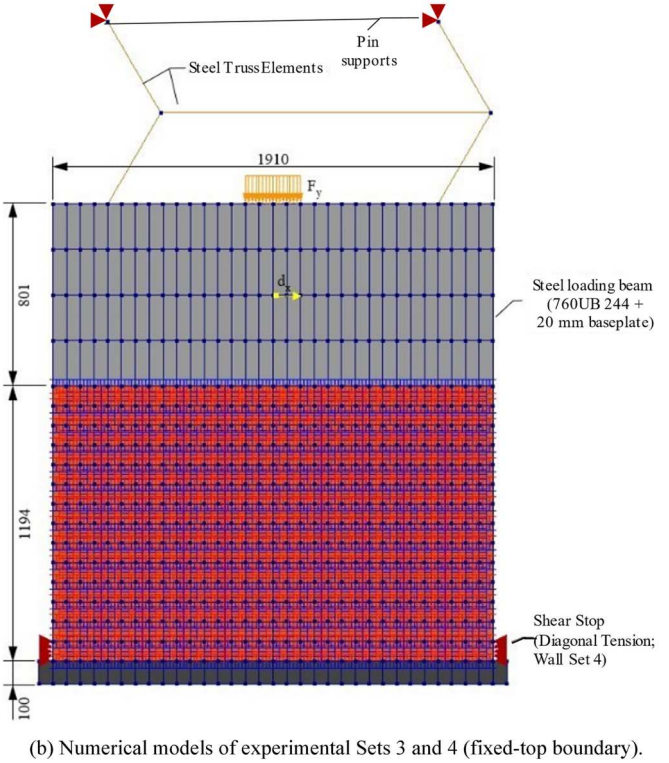

(b) Numerical models of experimental Sets 3 and 4 (fixed-top boundary).

Figure 1. Simplified FEA micro-models: (a) numerical models of experimental Sets 1 and 2 (cantilevered), and interface element breakdown and (b) numerical models of experimental Sets 3 and 4 (fixed-top boundary).

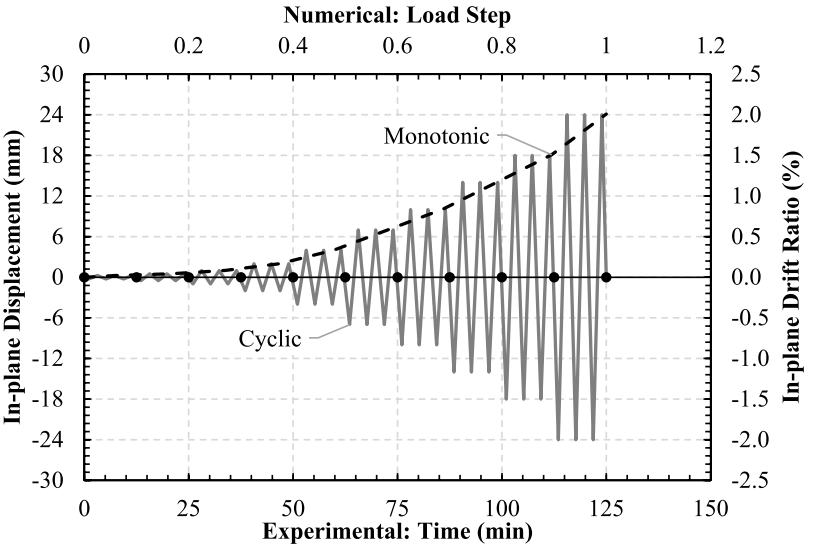

Figure 2. Comparison of monotonic and cyclic applications of shear displacements.

However, the monotonic loading scheme resulted in a significant overprediction of the peak in-plane shear capacity of walls subject to shear-based failure modes. As such, a cyclic displacement scheme, consistent with the experimental program, was adopted in the SFEAs to maximise accuracy, at the expensive of computational time.

2.3. Material models

The properties required to define the material models have been determined via laboratory testing (refer to Gooch et al. 2024) and from the literature noted in Table 1. Despite using a single type of masonry unit and a single mortar mixing ratio across the entire experimental testing program, the results of these material characterisation tests indicated that the initial division of specimens into four sets distinguished by their geometries and boundary conditions was insufficient. For example, in the case of Set 1, two mortar batches were utilised in the construction of the four wall specimens. Despite being constructed by the same mason and being tested after the same approximate curing period and in the same conditions, the first mortar batch maintained a flexural tensile bond strength equal to only one-third of that estimated for the second mortar batch. As such, this experimental set, and Sets 2 and 3, were further divided based upon these distinct material characteristics. The final set of SFEAs has been denoted as follows:

- Experimental Set 1 (flexural tension): SFEAs I and II
- Experimental Set 2 (flexural compression): SFEAs III and IV
- Experimental Set 3 (shear sliding): SFEAs V and VI, and
- Experimental Set 4 (diagonal tension): SFEA VII.

Table 2 presents a summary of the means and coefficients of variability (COVs) of the stochastic (randomly variable) material parameters adopted in this study's SFEAs. The PDFs determined to describe each parameter are derived by Gooch et al. (2024). These PDFs

Table 1. Summary of material parameters used in FE modelling.

Material	Property	Notation	Value	Unit	Source
Brick	Elastic modulus	E	26,315	N/mm^2	Compression test
	Poisson ratio	v	0.15	–	Heffler (2009)
	Mass density	ρ	1938	kg/m^3	AS 3700 (2018)
	Direct tensile strength	f_{bt}	Table 2	N/mm^2	Direct tension test
	Tensile fracture energy	$G^I_{f,unit}$	Equation (4)	Nmm/mm^2	Li (2015), after Lourenço et al. (2005)
Unit–mortar interface	Linear normal stiffness	k_n	Equation (1)	N/mm^3	Compression test, Mojsilović and Stewart (2015)
	Linear shear stiffness	k_s	Equation (2)	N/mm^3	
	Poisson ratio	v	0.20	–	Lourenço (1996a)
	Direct tensile strength	f_t	Table 2	N/mm^2	Bond wrench test
	Tensile fracture energy	$G^I_{f,joint}$	Equation (3)	Nmm/mm^2	Heffler (2009), after Van der Pluijm (1997)
	Shear bond strength	c	Table 2	N/mm^2	Triplet test
	Initial friction angle	ϕ_0	0.653	Radians	Confined triplet test
	Initial dilatancy angle	Ψ	0.464	Radians	Petersen (2009)
	Residual friction angle	ϕ_r	0.510	Radians	Masia et al. (2007)
	Dilatancy suppressing confining stress	σ_u	–0.75	N/mm^2	Petersen (2009)
	Shear bond degradation coefficient	δ	1.8	–	Petersen (2009)
	Masonry compressive strength	f_{uc}	Table 3	N/mm^2	Compression test
	Compressive fracture energy	G_{fc}	Equation (5)	Nmm/mm^2	Lourenço (1996a), after Model Code 90 (1991)
	Shear traction control factor	C_{ss}	9.0	–	Lourenço (1996a)
	Equivalent plastic relative displacement	κ_p	Equation (6)	mm	Lourenço (1996a), after Eurocode 6 (2005)
	Fracture energy factor (a)	G^{II}_f *(a)*	–0.49	mm	Petersen (2009)
	Fracture energy factor (b)	G^{II}_f *(b)*	0.035	Nmm/mm^2	Petersen (2009)
Steel	Elastic modulus	E	200 000	N/mm^2	AS4100 (1998)
	Poisson ratio	v	0.3	–	AS4100 (1998)
Concrete	Elastic modulus	E	30 100	N/mm^2	AS3600 (2018)
	Poisson ratio	v	0.2	–	AS3600 (2018)

Table 2. Summary of spatially variable material parameter statistics.

SFEA set[a]	Direct tensile unit strength f_{bt} (MPa)	Bed joint thickness $h_{j,bed}$ (mm)	Perpend joint thickness $h_{j,perpend}$ (mm)	Flexural tensile bond strength f_{mt} (MPa)	Shear bond strength c (MPa)
I *(1)*	1.53 [0.05]	10 [0.34]	10 [0.29]	0.27 [0.35]	0.42 [0.38]
II *(2)*				0.77 [0.31]	0.63 [0.16]
III *(3)*				0.47 [0.30]	0.32 [0.13]
IV *(4)*				0.25 [0.38]	0.41 [0.17]
V *(5, 6)*				0.40 [0.31]	0.81 [0.38]
VI *(7, 8)*				0.61 [0.18]	0.81 [0.38]
VII *(9–12)*				0.55 [0.24]	0.66 [0.23]

Note: COVs are shown in [ ].
[a]Relevant mortar batches from Gooch et al. (2024) are shown in ().

are: a Gumbel distribution for the direct tensile unit strength, a Lognormal distribution for the bed and perpend joint thicknesses and shear bond strength, and a Lognormal or Truncated Normal distribution for the flexural tensile bond strength. These findings are

Table 3. Summary of deterministic material parameters.

SFEA set	Masonry compressive strength f_{uc} (MPa)	Compressive fracture energy G_{fc} (Nmm/mm^2)	Masonry stiffness E_{mas} (MPa)	Mortar stiffness E_{mor} (MPa)
I, II	6.18	17.52	4328	589
III, IV	6.64	17.70	4650	641
V, VI	16.38	21.08	15543	4853
V	14.89	20.60	21,144	1496

consistent with the literature on masonry material behaviour (CEN 2002; Lawrence and Cao 1988; Lawrence and Lu 1991; Standards Australia 2018).

The masonry compressive strength, compressive fracture energy, and the stiffness of the mortar joints and composite masonry material have been adopted as deterministic properties. However, significant differences were observed between the measured masonry compressive strengths of specimens constructed by the different masons. As such, a different deterministic value for f_{uc}, G_{fc} (determined as per Equation 5), E_{mas} and E_{mor}, has been utilised for each SFEA depending on the mortar batch relevant to the modelled experimental specimens (refer to Table 3).

The linear normal (k_n) and shear (k_s) stiffnesses of the unit–mortar interface have been adopted as dependent random variables (see Equations 1 and 2), defined by a relationship between the thickness of the mortar joint (from the experimental data of Mojsilović and Stewart 2015), and the stiffness of the joint and adjacent masonry units; as proposed by Lourenço (1996a) and Rots (1997).

$$k_n = \frac{E_{\text{unit}} \cdot E_{\text{mor}}}{h_j \left(E_{\text{unit}} - E_{\text{mor}}\right)} \tag{1}$$

$$k_s = \frac{G_{\text{unit}} \cdot G_{\text{mor}}}{h_j \left(G_{\text{unit}} - G_{\text{mor}}\right)} \tag{2}$$

The Mode I fracture energies for both the unit–mortar interface ($G^I_{\text{f,joint}}$) and the unit cracking interface ($G^I_{\text{f,unit}}$) are estimated from deterministic relationships. These relationships directly relate the randomly variable direct tensile strength values to the fracture energy through empirical relationships. For the unit–mortar interface, Heffler (2009) proposed the linear relationship shown in Equation (3), based upon the experimental data presented by Van der Pluijm (1997), see Figure 3.

$$G^I_{f,\text{joint}} = 0.01571 f_t + 0.0004882 \tag{3}$$

Similarly, the tensile fracture energy of the masonry units may be estimated by the linear relationship to the direct tensile strength proposed by Li (2015) after the experimental work of Lourenço et al. (2005). This relationship is presented in Equation (4) and Figure 4.

$$G^I_{f,\text{unit}} = 0.0097 f_{bt} + 0.0277 \tag{4}$$

These models for fracture energy do not capture the high variability observable in the experimental results of Van der Pluijm (1997) and Lourenço et al. (2005). Li et al. (2016) note that the model error of Equations (3) and (4) (defined as the ratio between the experimental data and the corresponding model prediction) may be described utilising Lognormal distributions, with the means, μ_{ME}, and COVs, V_{ME}, shown in Figures 3 and 4.

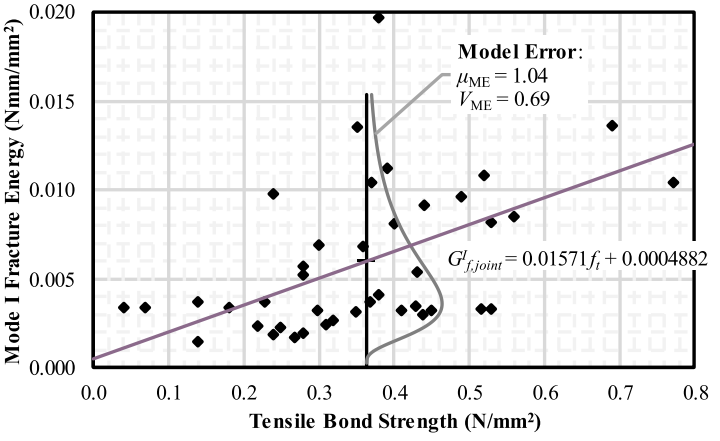

Figure 3. Tensile bond strength versus mode I fracture energy for clay brick masonry interface with general purpose mortar. Adapted from Heffler (2009).

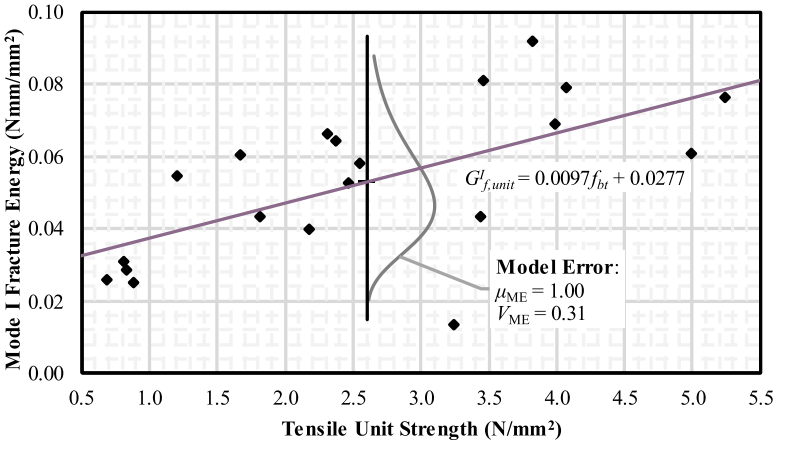

Figure 4. Tensile unit strength versus mode I fracture energy for clay bricks. Adapted from Li (2015).

Furthermore, the compressive fracture energy of the unit–mortar interface is also considered a dependent random variable, as this property is estimated through a deterministic relationship to the masonry compressive strength (see Equation 5), based upon the recommendations by Lourenço (1996a) after Model Code 90 for concrete (Comite Euro-International Du Beton 1991).

$$G_{fc} = -0.0036 f_{uc}^2 + 0.43 f_{uc} + 15 \tag{5}$$

The equivalent plastic relative displacement of the peak compressive strength (κ_p) may also be calculated as per Equation (6). This expression limits the compressive masonry strain to –0.002, as specified by Eurocode 6 (British Standards Institution 2005).

$$\kappa_p = \left\{ 0.002 - f_{uc} \left[\frac{1}{E_{unit}} + \frac{1}{k_n (h_{unit} + h_{joint})} \right] \right\} f_{uc} \tag{6}$$

2.4. Spatial variability

Previous studies considering the spatial variability of the joint-to-joint flexural tensile bond strength of bed joints (Isfeld et al. 2021, 2023; Li et al. 2016; Muhit 2021) have adopted a correlation coefficient (ρ_k) of 0.40, after the results of Heffler et al., (2008). Furthermore, Heffler et al., (2008) found that no significant correlation exists between adjacent perpend joints, nor between the bed or perpend joints of successive courses, i.e. $\rho_k = 0$. Hence, these values have been adopted for the current study.

In the case of the shear bond strength of mortar joints, a correlation coefficient between the flexural tensile and shear bond strengths of a single joint equal to 0.75 has been derived by Gooch et al., (2023). Furthermore, considering the experimental data by Mojsilović and Stewart (2015), no statistically significant correlation between adjacent or successive perpend or bed joint thicknesses was found. This finding is consistent with the data presented by Farjada and Shrive (2023).

3. SFEA results

The experimentally observed in-plane shear capacities, as well as the corresponding failure mechanisms, facilitate the quantification of the ME of each SFEA's estimate of in-plane shear capacity. The initial 15 Monte-Carlo simulations were utilised in SFEAs I to VI. This number was selected to balance the high computational expense of the implemented cyclic loading scheme and the need for a stable estimate of the mean and COV of the in-plane shear strength (i.e. converged to an accuracy of ±1.0% for the mean and ±0.005 for the COV). However, as shown in Table 4, SFEAs III and VI utilised an additional five simulations to ensure a stable estimate of the COV of the peak in-plane shear strength. Furthermore, 25 simulations were adopted for SFEA VII due to the larger number of experimental wall specimens and the higher observed experimental COV.

3.1. SFEAs I and II – 0.5 MPa, AR: 1.0, cantilevered

The dominant failure mechanism predicted by SFEAs I and II was a flexural tensile failure mode. This mechanism is consistent with the experimental observations by Gooch et al. (2024). Cracking was generally limited to the bottom one or two courses of bed joints, as shown in Figures 5(a) and (d). However, some predicted cracking was consistent with the stepped diagonal cracks observed for experimental specimen Wall 2 of Set 1, (see

Table 4. Summary of SFEA configurations.

SFEA	Number of simulations	Exp. wall specimens	Aspect ratio	Pre-compression (MPa)	In-plane rotational restraint	Expected failure mode(s)[a]
I	15	I-1, I-2	1.0	0.5	Cantilevered	FT
II	15	I-3, I-4	1.0	0.5	Cantilevered	FT
III	20	II-1, II-2	1.0	1.0	Cantilevered	FT/FC
IV	15	II-3, II-4	1.0	1.0	Cantilevered	FT/FC
V	15	III-1, III-2	0.625	0.5	Fixed–fixed	SS/DT
VI	20	III-3, III-4	0.625	0.5	Fixed–fixed	SS/DT
VII	25	IV-1 to IV-4	0.625	0.7	Fixed–fixed	SS/DT

[a]Flexural tension (FT), Flexural compression (FC), Shear sliding (SS), Diagonal tension (DT).

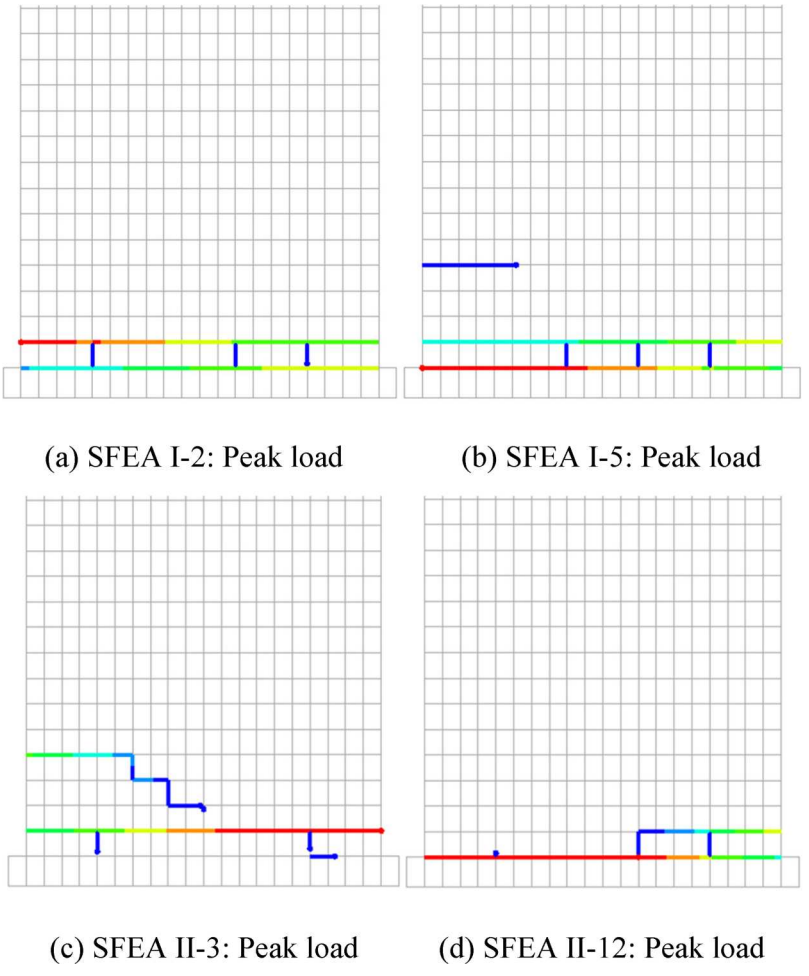

Figure 5. Predicted crack patterns at peak in-plane shear capacity, representative of typical SFEAs I and II realisations, illustrated by normalised crack widths determined by each simulation: (a) SFEA I-2: peak load; (b) SFEA I-5: peak load; (c) SFEA II-3: peak load and (d) SFEA II-12: peak load.

Figure 5b). Furthermore, the examination of the interface normal stresses of each simulation indicates that none of the simulations experienced a compressive failure at the point of peak shear capacity.

The mean peak in-plane shear strength, averaged from both the positive and negative loading directions are presented in Figure 6, along with the observed failure mechanism of each individual Monte-Carlo realisation.

The load–displacement envelopes of SFEAs I and II have been compared to the corresponding experimental results by Gooch et al. (2024). Each SFEA predicted a high initial stiffness, comparable to the experimental specimens, with the peak in-plane shear strength predicted between approximately 1.5 and 6 mm of in-plane displacement. However, the post-peak responses were not captured as accurately. The post-peak strength decrease in shear strength was predicted to be larger than in the experimental specimens (see Figure 7). Furthermore, the failure of the structure defined as a 20%

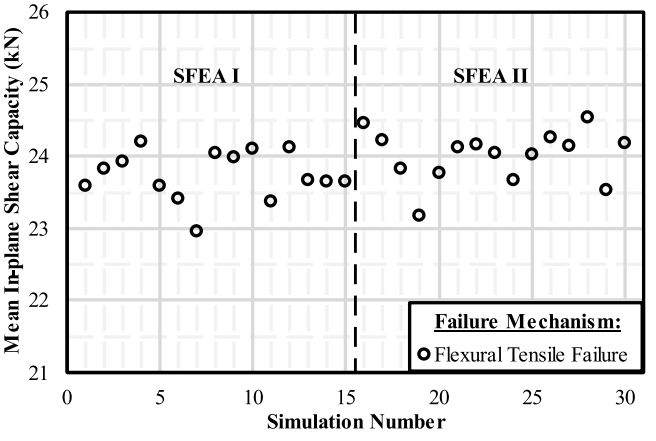

Figure 6. Mean shear strengths and failure mechanisms of SFEAs I and II.

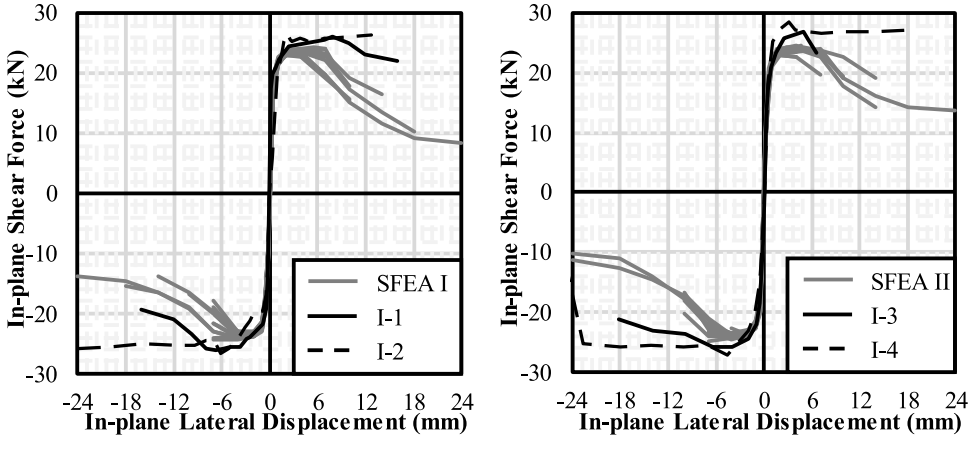

Figure 7. Lateral load–displacement response of SFEAs I and II and experimental Wall Set 1.

decrease in post-peak load carrying capacity (ASTM International 2011; Magenes et al. 2008; Tomaževič 1999), was estimated to occur between 4 and 10 mm of in-plane displacement, in contrast, to the experimentally observed range of 12 to 24 mm. Despite this poorer post-peak representation, a clear estimate of the peak shear capacity is obtainable for each SFEA, allowing for a confident numerical estimation of the mean load carrying capacity.

The mean shear strengths determined from SFEAs I and II were 23.7 and 24.0 kN, with COVs 0.014 and 0.015, respectively. These values when compared to the experimental baselines produce average errors of 10.1% and 11.5%, for SFEAs I and II, respectively. These results are summarised in Table 5.

3.2. SFEAs III and IV – 1.0 MPa, AR: 1.0, cantilevered

The dominant failure mechanism predicted by the realisations of SFEAs III and IV was that of either a flexural tension or flexural compression failure. This is characterised by the

Table 5. Comparison for SFEA I and II versus experimental Wall Set 1.

		SFEA results			Exp. value			
SFEA	Parameter	Mean	COV	Exp. wall specimen	Pull (+)	Push (–)	Exp. mean	%Diff[a]
I	V_{max} (kN)	23.7	0.014	I-1	26.2	26.1	26.4	10.11%
				I-2	26.7	26.6		
	δ_{Vmax} (mm)	4.7	0.267	I-1	7.9	6.8	5.7	17.84%
				I-2	2.1	6.1		
	δ_u (mm)	9.6	0.557	I-1	15.9	12.2	16.2	40.54%
				I-2	12.7	24.0		
II	V_{max} (kN)	24.0	0.015	I-3	26.9	25.9	27.1	11.50%
				I-4	28.6	27.2		
	δ_{Vmax} (mm)	4.1	0.646	I-3	4.9	3.9	3.9	−5.76%
				I-4	2.1	4.7		
	δ_u (mm)	10.0	0.329	I-3	6.5	18.1	16.5	39.61%
				I-4	18.2	23.2		

[a]Percentage difference between the experimental value and the numerical prediction.

presence of flexural cracking in the first three courses of bed joints, often accompanied by damage to perpend joints at the base of wall, see Figures 8(a) and (b).

The distribution of compressive stresses was examined to separate flexural tension and compression failures. At the point of peak in-plane shear strength, compressive stresses decreased linearly from the toe of the wall, typical of either flexural failure (see Figure 9a). However, in cases where a flexural compression failure was predicted, the masonry compression strength was reached at the point of peak in-plane shear capacity. Furthermore, the following cycles predict the peak compressive stresses away from the toe of the wall (see Figure 9b). These stress distributions are the result of the reduction of effective compressive strength in accordance with the adopted compressive cap model (Lourenço 1996b) once the initial masonry compression strength is exceeded.

These predictions are consistent with the experimental observations and facilitate an accurate determination of the failure mechanism of each SFEA realisation, as presented in Figure 10.

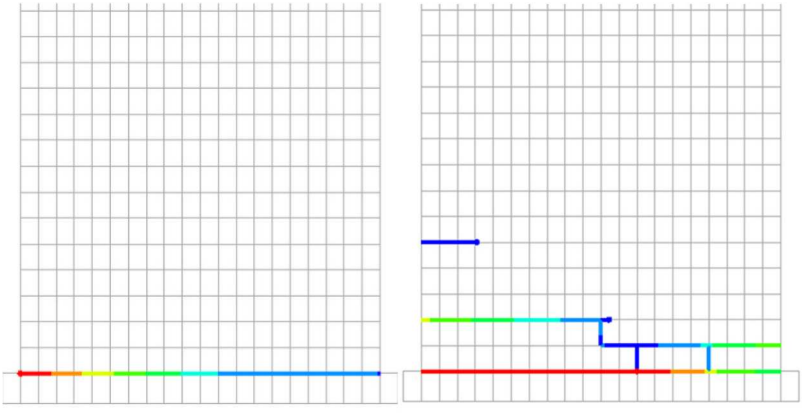

(a) SFEA III-9: Peak Load (b) SFEA IV-2: Peak Load

Figure 8. Predicted crack patterns at the peak in-plane shear capacity, representative of typical SFEA III and IV realisations, illustrated by normalised crack widths determined by each simulation: (a) SFEA III-9: peak load and (b) SFEA IV-2: peak load.

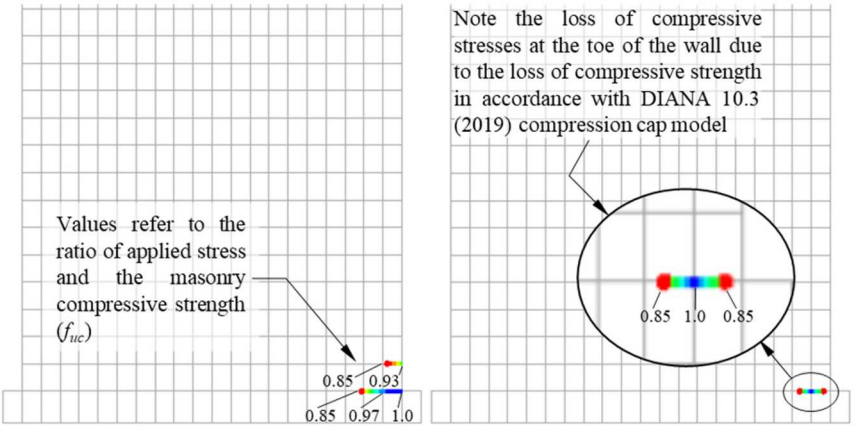

(a) SFEA III-2: Compressive stresses at the peak in-plane shear capacity.

(b) SFEA III-2: Compressive stresses one displacement cycle post-peak.

Figure 9. Predicted compressive stresses near the masonry compressive strength at and beyond peak in-plane shear capacity, representative of typical SFEA III and IV realisations: (a) SFEA III-2: compressive stresses at the peak in-plane shear capacity and (b) SFEA III-2: compressive stresses one displacement cycle post-peak.

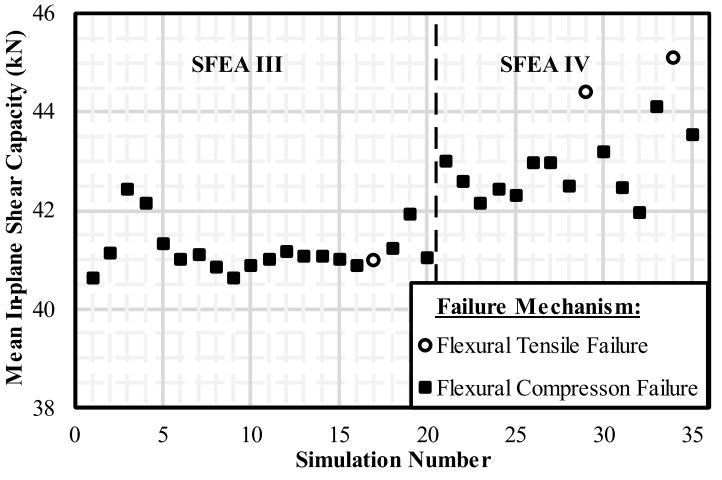

Figure 10. Mean shear strengths and failure mechanisms of SFEAs III and IV.

The load–displacement responses predicted by SFEAs III and IV are compared to the laboratory results in Figure 11. The envelopes of the SFEAs exhibit a high initial stiffness followed by a decrease in in-plane shear capacity. While the predicted values of δ_{Vmax} are lower than the experimental baselines, the overall response is consistent with Gooch et al. (2024). Furthermore, predictions of the in-plane shear strength were consistent with experimental observations, with average errors of 9.75% and 6.20%, respectively (Table 6).

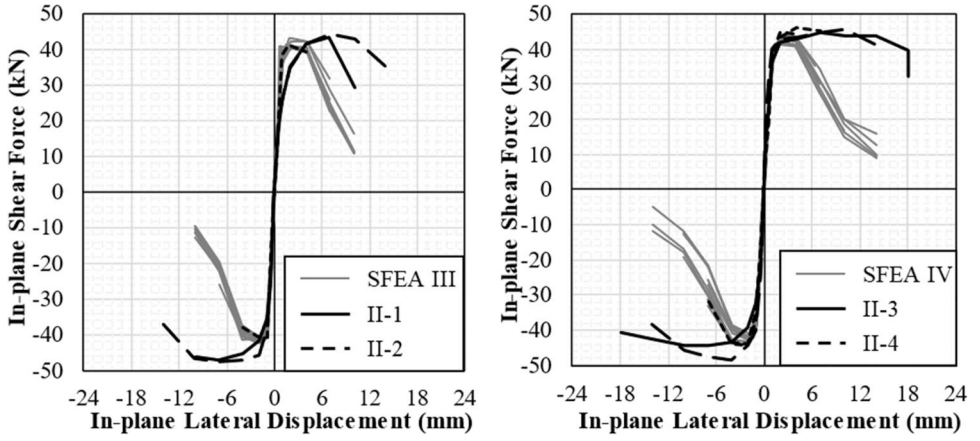

Figure 11. Lateral load–displacement response of SFEAs III and IV and experimental Wall Set 2.

Table 6. Comparison for SFEAs III and IV versus experimental Wall Set 2.

		SFEA results			Exp. value			
SFEA	Parameter	Mean	COV	Exp. wall specimen	Pull (+)	Push (–)	Exp. mean	%Diff[a]
III	V_{max} (kN)	41.2	0.011	II-1	43.4	47.1	45.6	9.75%
				II-2	44.3	47.7		
	δ_{Vmax} (mm)	1.7	0.472	II-1	6.9	7.0	7.0	76.31%
				II-2	7.1	7.0		
	δ_u (mm)	6.7	0.393	II-1	8.8	9.9	11.6	42.17%
				II-2	14.0	13.6		
IV	V_{max} (kN)	43.0	0.021	II-3	44.8	44.6	45.9	6.20%
				II-4	45.6	48.6		
	δ_{Vmax} (mm)	2.3	0.454	II-3	7.0	10.1	7.8	70.05%
				II-4	10.0	4.0		
	δ_u (mm)	9.0	0.254	II-3	18.0	18.0	16.0	44.04%
				II-4	14.1	13.8		

[a]Percentage difference between the experimental value and the numerical prediction.

3.3. SFEAs V and VI – 0.5 MPa, AR: 0.63, fixed–fixed

The predicted failure modes of SFEAs V and VI (see Figure 12) are consistent with the experimental results reported by Gooch et al. (2024). In addition to the predicted crack patterns, the load–displacement behaviour of each SFEA realisation was investigated to accurately determine the governing failure mechanism.

A limitation of SFEAs V and VI is the overestimation of the stiffness prior to the predicted peak shear strength. This introduces uncertainty when determining the failure mechanism from the crack patterns alone as the peak shear strengths were predicted at in-plane displacements between 0.2 and 0.5 mm. Due to this high initial stiffness, crack widths are limited at the point of peak strength, as seen in Figure 13. However, the formation of a single clear sliding plane was evident in predicted shear sliding failures, even at small in-plane displacements. These planes occurred predominantly through the first and second courses (see Figures 13a and b). Conversely, for diagonal tensile failures, a larger number of often less distinct sliding planes were predicted (see Figure 13c).

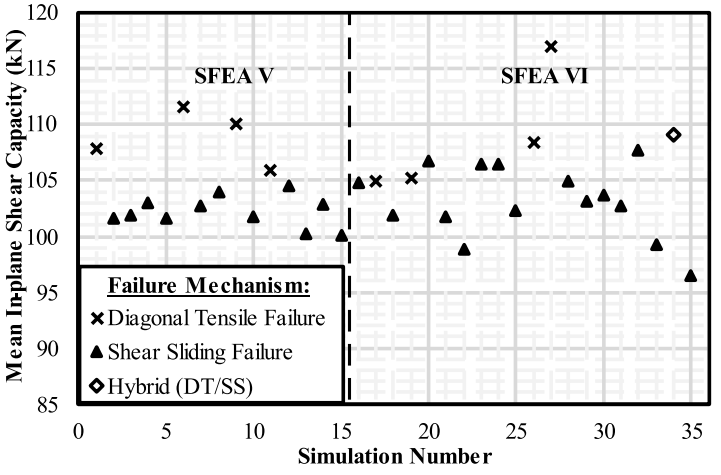

Figure 12. Mean shear strengths and failure mechanisms of SFEAs V and VI.

However, as shown in Figure 13(d), these planes were not always significantly distinct from a shear sliding failure at low in-plane displacements.

The load–displacement responses of the SFEAs are presented against the experimentally observed responses in Figure 14. The mean differences in the predictions of shear

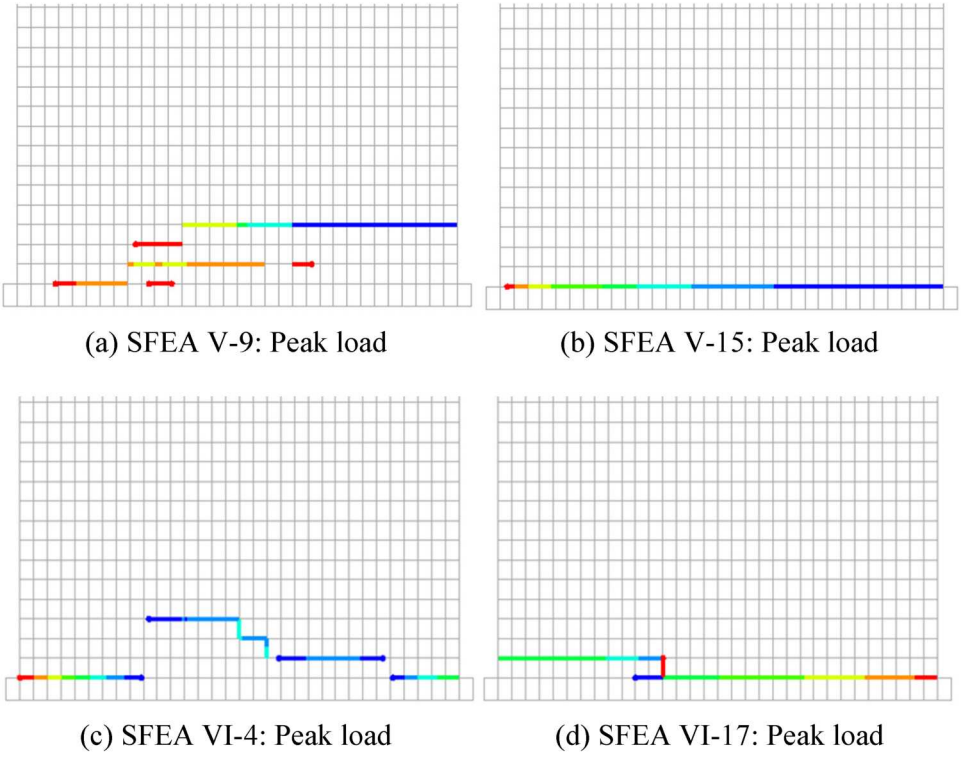

Figure 13. Predicted crack patterns at peak in-plane shear capacity, representative of typical SFEA V and VI realisations, illustrated by normalised crack widths determined by each simulation: (a) SFEA V-9: peak load; (b) SFEA V-15: peak load; (c) SFEA VI-4: peak load and (d) SFEA VI-17: peak load.

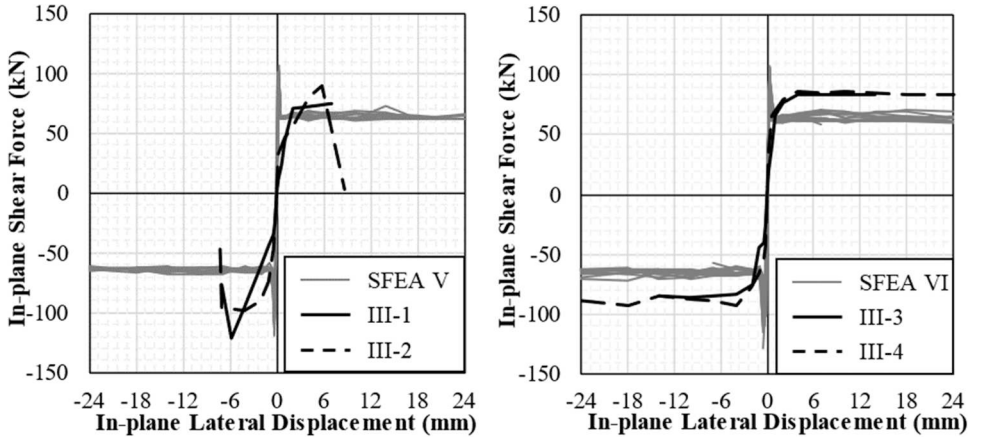

Figure 14. Lateral load–displacement response of SFEAs V and VI and experimental Wall Set 3.

capacity between SFEAs V and VI and the experimental walls are −8.27% and −20.57%, respectively. While these errors in the predictions of in-plane shear capacity are consistent with previous studies of URM shear walls (Howlader et al. 2020; Konthesingha 2012), the shapes of the hysteretic envelopes are significantly different to experimental observations. This discrepancy is a result of the overestimation of the initial stiffness of the modelled wall specimens in DIANA 10.3. The effect of this overestimation is exacerbated by the apparent bilinear stiffness observed in the experimental walls (refer to Figure 14a). Many permutations of the adopted modelling strategy were trialled to address this issue; however, these alterations produced minimal variations in the predicted results and were not capable of capturing the bilinear stiffness observed experimentally (see Table 7).

3.4. SFEA VII – 0.7 MPa, AR: 0.63, fixed–fixed

The failure modes predicted by SFEA VII (summarised in Figure 15) were consistent with the mix of shear-based failure modes observed during laboratory testing. The predicted

Table 7. Comparison for SFEAs V and VI versus experimental Wall Set 3.

		SFEA results			Exp. value			
SFEA	Parameter	Mean	COV	Exp. wall specimen	Pull (+)	Push (–)	Exp. mean	%Diff[b]
V	V_{max} (kN)	104.0	0.033	III-1	75.0	120.7	96.0	−8.27%
				III-2	90.5	97.9		
	δ_{Vmax} (mm)	0.25	0.0[a]	III-1	7.1	5.8	5.7	95.61%
				III-2	5.8	4.1		
	δ_u (mm)	15.8	0.641	III-1	7.1	6.5	6.8	−134.61%
				III-2	6.4	7.1		
VI	V_{max} (kN)	105.5	0.039	III-3	84.2	86.2	87.5	−20.57%
				III-4	86.2	93.3		
	δ_{Vmax} (mm)	0.3	0.720	III-3	4.0	9.9	5.5	94.37%
				III-4	4.0	4.1		
	δ_u (mm)	15.4	0.340	III-3	14.0	14.0	19.0	19.00%
				III-4	24.1	23.9		

[a]A COV of 0.0 was determined for δ_{Vmax} as all values of V_{max} were predicted at $\delta = 0.25$ mm.
[b]Percentage difference between the experimental value and the numerical prediction.

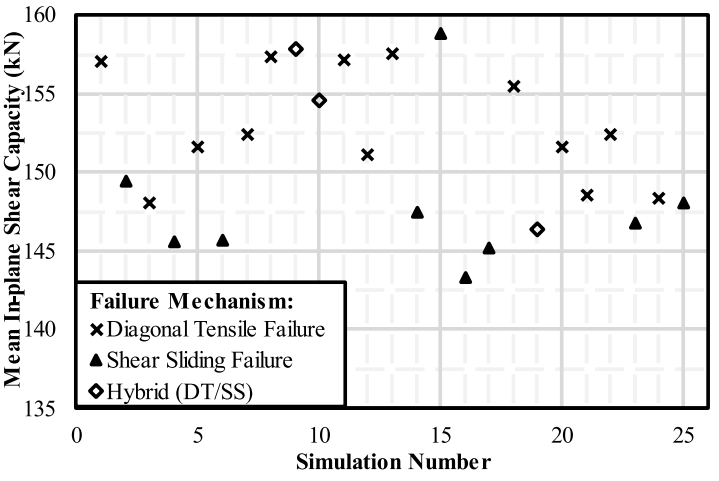

Figure 15. Mean shear strengths and failure mechanisms of SFEA VII.

failure mechanisms could typically be determined from the predicted crack patterns and were confirmed through the investigation of the predicted load–displacement behaviours and the ultimate displacements of the SFEA realisations.

Predicted diagonal tensile failures produced a series of characteristic stepped cracks through the bed and perpend joints of the wall (see Figure 16b), while shear sliding failures were identifiable by the formation of sliding planes, (refer to Figure 16a). Furthermore, hybrid failure modes were discernible by the formation of several staggered sliding planes that subsequently produced a diagonal tension failure surface via the propagation of damage under cyclic loading (refer to Figures 16c and d).

The load–displacement behaviours predicted by SFEA VII exhibit the same issue as SFEAs V and VI, displaying a difference between the initial stiffnesses of the numerical models and laboratory specimens. This is a result of the bilinear stiffness observed in the laboratory tests (Gooch et al. 2024). Despite this limitation, SFEA VII produced an accurate estimation of the peak strength. A prediction of V_{max} of 151.1 kN with a COV of 0.031 was determined from SFEA VII. This corresponds to an average error of 4.18% (Figure 17) (Table 8).

3.5. Limitations

To address the limitations observed in the predictions of each SFEA (particularly those that produced shear-based failure mechanisms), an extensive sensitivity analysis was performed. These analyses considered the sensitivity of results to:

- Meshing techniques: linear and higher-order elements, triangular and rectangular elements, mesh density, etc.
- Material properties: aggregated from a larger sample of the testing data of Gooch et al. (2024), values taken from the literature (Lawrence 1983; Lourenço 1996a; McNeilly et al. 1996), upper-and-lower bound percentiles (60%, 70%, 85%, 95% and 99%) of properties in deterministic FEMs, and extreme values of insensitive parameters.

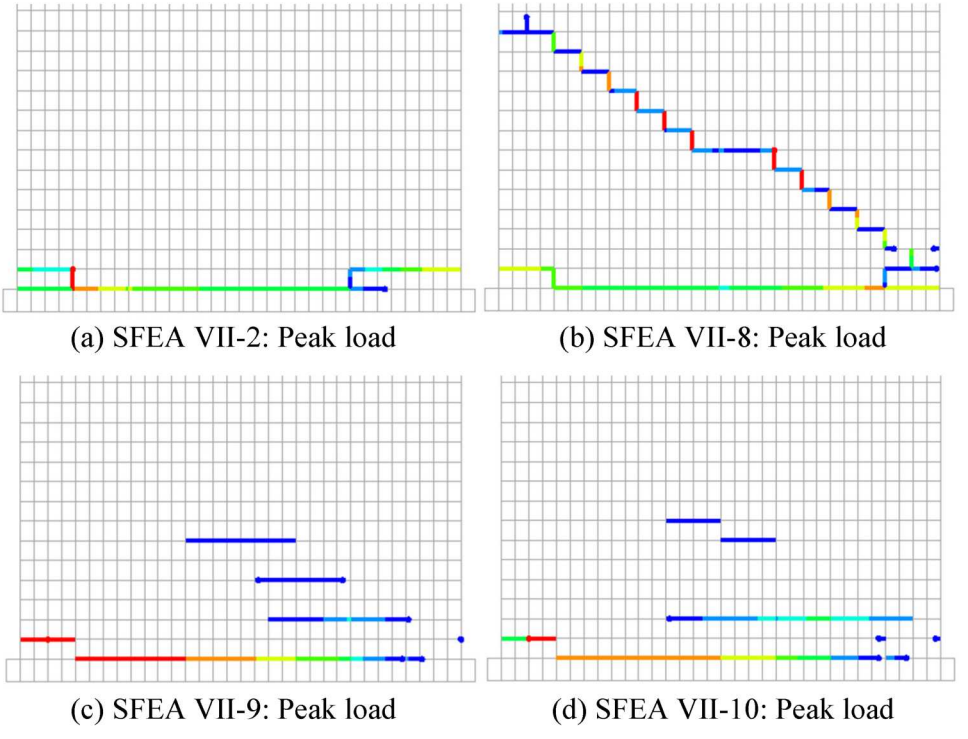

Figure 16. Predicted crack patterns at peak in-plane shear capacity, representative of typical SFEA VII realisations, illustrated by normalised crack widths determined by each simulation: (a) SFEA VII-2: peak load; (b) SFEA VII-8: peak load; (c) SFEA VII-9: peak load and (d) SFEA VII-10: peak load.

These analyses were applied to a large number of permutations of each of the previously discussed SFEAs, as well as to deterministic equivalents. The final modelling technique presented in this study is the culmination of this investigation, the results of which indicate that the capture of this complex shear failure behaviour is beyond the capacity of the adopted FEM method.

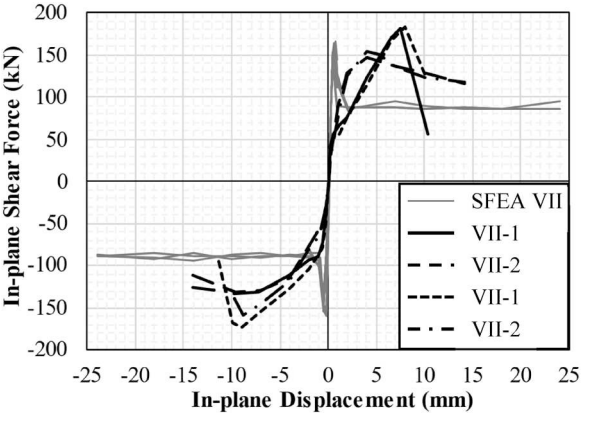

Figure 17. Lateral load–displacement response of SFEA VII and experimental Wall Set 4.

Table 8. Comparison for SFEA VII versus experimental Wall Set 4.

	SFEA results			Exp. value			
Parameter	Mean	COV	Exp. wall specimen	Pull (+)	Push (–)	Exp. mean	%Diff[a]
V_{max} (kN)	151.1	0.031	IV-1	181.8	133.5	157.7	4.18%
			IV-2	147.5	131.7		
			IV-3	182.8	172.4		
			IV-4	153.8	158.3		
δ_{Vmax} (mm)	0.6	0.254	IV-1	7.5	9.8	7.6	92.75%
			IV-2	4.0	9.6		
			IV-3	8.0	9.0		
			IV-4	4.0	8.8		
δ_u (mm)	3.8	2.041	IV-1	8.3	9.8	11.1	66.29%
			IV-2	13.4	14.0		
			IV-3	9.3	10.5		
			IV-4	10.7	13.0		

[a]Percentage difference between the experimental value and the numerical prediction.

4. SFEA model error

From the results presented in Section 3, the ME associated with each SFEA can be investigated. The ME of interest is that related to the SFEA predictions of the shear force required to initiate the distinct failure mechanisms of URM shear walls examined in this study; noted in the previous sections as the mean peak in-plane shear forces. The ME for each failure mode is

$$\text{ME} = \frac{\text{Average experimental capacity}}{\text{Model predicted capacity}} \tag{7}$$

where the *Average experimental capacity* is the average of the peak in-plane shear strengths recorded experimentally in both the push (–) and pull (+) directions for all nominally identical experimental wall specimens, and the *Model predicted capacity* is the average shear strength in the push and pull directions of a corresponding SFEA realisation.

The variability of the data determined from Equation (7) is a suitable proxy from which the normalised variability of the SFEA predictions of peak strength (V_{SFEA}) may be determined. The variability of ME (V_{ME}) is then determined as a function of V_{SFEA} and of the variability of the experimentally determined shear capacities ($V_{Exp.}$), and is calculated as

$$V_{ME} = \sqrt{V_{Exp.}^2 - V_{SFEA}^2} \tag{8}$$

Further to this, $V_{Exp.}$ is determined from experimentally measured variability ($V_{measured}$), as presented by Gooch et al. (2024), the variability introduced into the laboratory testing as a result of inaccuracies in the gauges, reading outs and definitions of values (V_{test}), and variability caused by differences between strengths or geometries in the experimental and control test specimens (V_{spec}) (Ellingwood et al. 1980), as

$$V_{Exp.} = \sqrt{V_{measured}^2 - V_{test}^2 - V_{spec}^2} \tag{9}$$

Values of $V_{measured}$ equal to 0.029 and 0.020 were observed for flexural tension and flexural compression failures, respectively (note that the value of 0.020 was derived from only two data points, and thus may be unreliable. However, this value of 0.020 is

Table 9. Measured variabilities of peak in-plane shear strength, $V_{measured,}$ for each failure mechanism.

Failure mode	Experimental set	Sample size	$V_{measured}$
Flexural tension	I	4	0.029
Flexural compression	II	2	0.020
Shear sliding	III	3	0.050
Diagonal tension	IV	4	0.099

consistent with the overall variability of Set II equal to 0.022 (Gooch et al. 2024)). These values are consistent with expectations, considering typical mean values and variabilities for masonry material properties (Lawrence 1983; McNeilly et al. 1996; Stewart and Lawrence 2007; Petersen et al. 2008), as well as the design equations presented in CSA S304-14 (2014), NZSEE (2017), AS 3700 (2018) and TMS 402/602-22 (2022). Similarly, values of $V_{measured}$ equal to 0.050 and 0.099 have been determined for shear sliding and diagonal tension failures. However, due to the evidence of hybridisation reported by Gooch et al. (2024), further investigation into the variability of these failure modes is recommended. These adopted values of $V_{measured}$ are summarised in Table 9.

It should also be noted that, although the laboratory testing of 16 full-scale wall specimens and the associated material characterisation tests performed by Gooch et al. (2024) was significant in scope, it amounts to few datapoints relevant to the analysis performed herein. Though the application of synthetic data generation is intended to offset these limitations, the small sample size from which ME can be derived in the current study predicates that the findings below are only indicative of the adopted FEM technique.

4.1. Mean model error and SFEA variability

The following sections outline the derivation of suitable probabilistic models that describe the ME of each SFEA's prediction of the shear resistance for each of the examined failure mechanisms. These models have been derived by fitting Weibull, Normal, Lognormal, Gamma and Gumbel distributions to values of ME, and considering both the results of Kolmogorov–Smirnov (K–S) and Anderson–Darling (A–D) tests, and the goodness-of-fit of each distribution.

4.1.1. Flexural tension

A flexural tensile failure mode was predicted by all realisations of SFEAs I and II. Furthermore, there is good agreement in the values of ME between these two analyses, as shown in Figure 18, with mean MEs equal to 1.11 and 1.13 for SFEAs I and II, respectively. From these results, values of $\mu_{ME} = 1.13$ and $V_{SFEA} = 0.017$ have been determined for the prediction of flexural tension failures.

None of the probabilistic models could be rejected at the 5% significance level by either the K–S or A–D tests. As such, a qualitative assessment of the goodness-of-fit of each distribution has been performed. As may be observed in Figure 19(b), the Weibull, Normal and Lognormal distributions produce results closest to the line of perfect fit across the entire domain. Furthermore, the Lognormal model produces the best fit to the data at the lower tail of the CDF^{-1}. Accuracy in this region is of the highest significance to a reliability analysis as it corresponds to a weaker than average ultimate resistance, and thus to a structural element with a greater probability of failure.

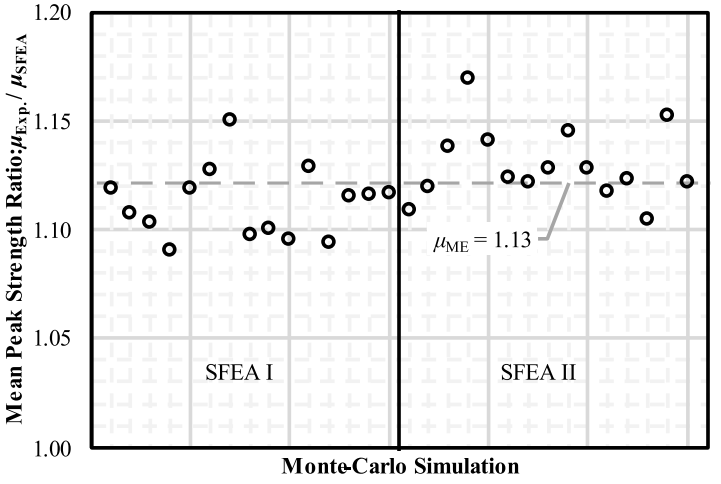

Figure 18. Distribution of the ratio between experimental and SFEA peak strengths for flexural tensile failures.

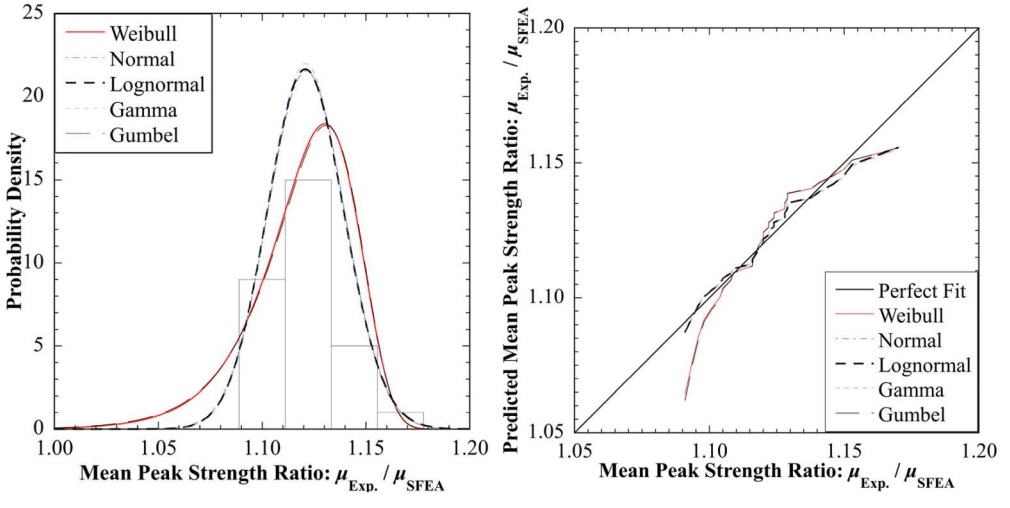

(a) PDFs of Mean Peak Strength Ratio: $\mu_{Exp.}$ / μ_{SFEA} (Flexural Tension)

(b) CDF^{-1}s of Mean Peak Strength Ratio: $\mu_{Exp.}$ / μ_{SFEA} (Flexural Tension)

Figure 19. Probabilistic distributions and inverse CDF plots of the ratio between mean experimental and SFEA peak strength for flexural tensile failures: (a) PDFs of mean peak strength ratio: $\mu_{Exp.}/\mu_{SFEA}$ (Flexural Tension) and (b) CDF^{-1}s of mean peak strength ratio: $\mu_{Exp.}/\mu_{SFEA}$ (Flexural Tension).

Hence, a Lognormal distribution has been adopted for the ME of predicting a flexural tension failure.

4.1.2. Flexural compression

Flexural compression failures were predicted by SFEAs III and IV. A comparison to the experimental observations is presented in Figure 20 and facilitates the determination

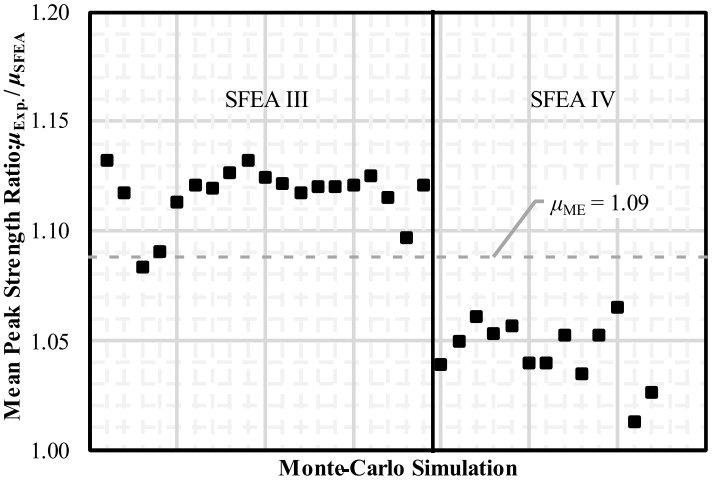

Figure 20. Distribution of the ratio between mean experimental and SFEA peak strength for flexural compressive failure modes.

of a mean ME for the prediction of a flexural compressive failure resistance of $\mu_{ME} = 1.09$, with $V_{SFEA} = 0.035$.

The goodness-of-fit of each distribution presented in Figure 21 indicates that the Log-normal distribution produces a more accurate fit to the middle and lower tails of the CDF^{-1}. As such, this probabilistic distribution has been adopted to describe the ME of the SFEAs that describe a flexural compressive failure.

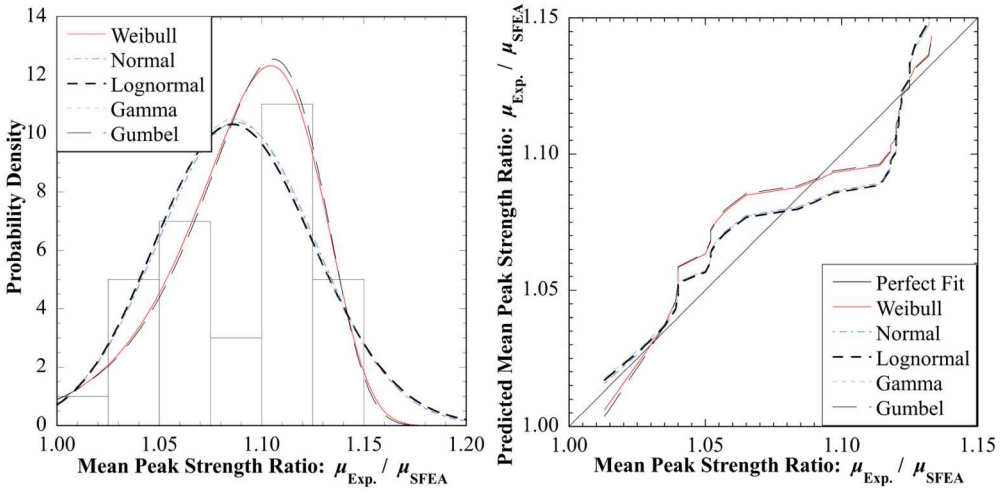

(a) PDFs of Mean Peak Strength Ratio: $\mu_{Exp.} / \mu_{SFEA}$ (Flexural Compression)

(b) CDF^{-1}s of Mean Peak Strength Ratio: $\mu_{Exp.} / \mu_{SFEA}$ (Flexural Compression)

Figure 21. Probabilistic distributions and inverse CDF plots of the ratio between mean experimental and SFEA peak strength for flexural compressive failures: (a) PDFs of mean peak strength ratio: $\mu_{Exp.}/\mu_{SFEA}$ (Flexural Compression) and (b) CDF^{-1}s of mean peak strength ratio: $\mu_{Exp.}/\mu_{SFEA}$ (Flexural Compression).

4.1.3. Shear sliding

The results of SFEAs V, VI and VII all contain predictions of the shear sliding failure loads. From the results of SFEAs V, VI and VII, mean MEs of 0.92, 0.85 and 1.06 were determined, respectively. These notably distinct means are evident in Figure 22, and are a result of the limitations discussed in Sections 3.3 and 3.4. While the overall mean $\mu_{ME} = 0.94$ is indicative of an accurate representation of the experimentally observed response, the inconsistencies evident between SFEAs are reflected in the larger $V_{SFEA} = 0.10$. Due to this observation, as well as issues with load–displacement predictions, these results should be considered with caution. Refinement of the numerical and experimental modelling of walls subject to shear-based failure modes is planned in future studies.

From Figure 23(b), it may be observed that the Lognormal distribution produces the most accurate fit to most of the presented data and is slightly more conservative than the fitted Normal distribution. Hence a Lognormal distribution may be adopted to describe ME for the SFEAs that produce a shear sliding failure.

4.1.4. Diagonal tension

SFEA V produced four Monte-Carlo simulations that predicted a diagonal tensile failure, resulting in a mean ME of 0.90, while SFEA VII predicted 13 diagonal tensile failures, with a mean ME of 1.03. The overall average ratio between the SFEAs and the experimental wall specimens that produced a diagonal tensile failure $\mu_{ME} = 1.00$ and a value of $V_{SFEA} = 0.062$. This indicates that, on average, the numerical models presented in this study produce near perfect predictions of the shear resistances of the experimental walls that experienced a diagonal tensile failure. However, the limited accuracy in the predictions of the load–displacement responses (see Sections 3.3 and 3.4) indicates that these findings, as with those for shear sliding, should be utilised with a degree of caution.

The ME associated with a diagonal tensile failure has been derived from relatively few values. Despite this limitation, Figure 25(b) shows that the Normal, Lognormal and Gamma distributions produce a conservative fit to the data for values less than

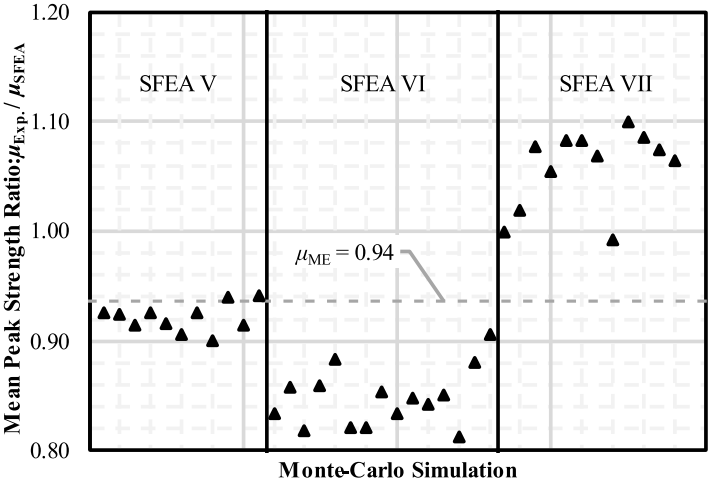

Figure 22. Distribution of the ratio between mean experimental and SFEA peak strength for shear sliding failure modes.

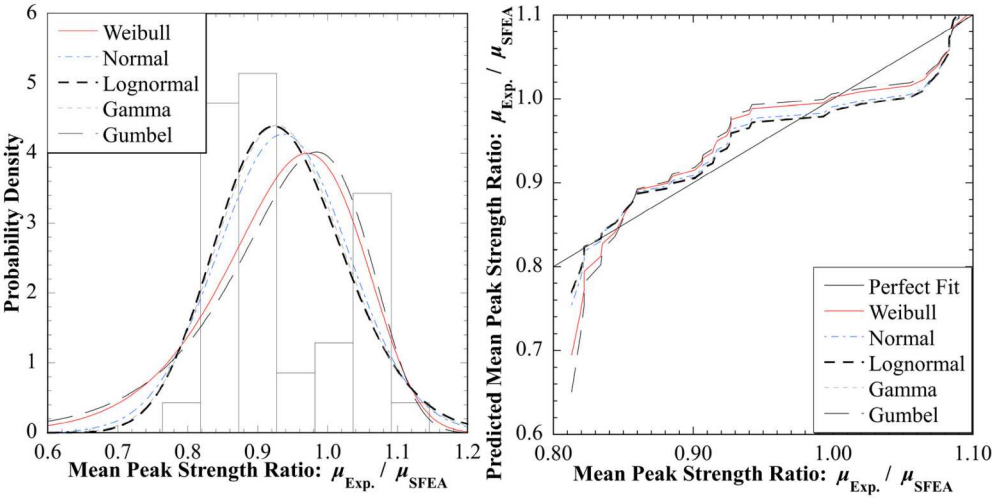

(a) PDFs of Mean Peak Strength Ratio: $\mu_{Exp.}$ / μ_{SFEA} (Shear Sliding)

(b) CDF^{-1}s of Mean Peak Strength Ratio: $\mu_{Exp.}$ / μ_{SFEA} (Shear Sliding)

Figure 23. Probabilistic distributions and inverse CDF plots of the ratio between mean experimental and SFEA peak strength for shear sliding failures: (a) PDFs of mean peak strength ratio: $\mu_{Exp.}/\mu_{SFEA}$ (Shear Sliding) and (b) CDF^{-1}s of mean peak strength ratio: $\mu_{Exp.}/\mu_{SFEA}$ (Shear Sliding).

approximately 1.05, with a Lognormal model producing the most accurate fit to the data shown in Figure 24. As such, a Lognormal distribution may be adopted to describe the ME for SFEAs prediction of a diagonal tensile failure load (Figure 25).

4.1.5. Summary of mean ME and SFEA variability by failure mode

From the results presented above, values of V_{SFEA} have been derived for each of the observed failure mechanisms. Furthermore, a mean value of ME, μ_{ME}, as well as a suitable

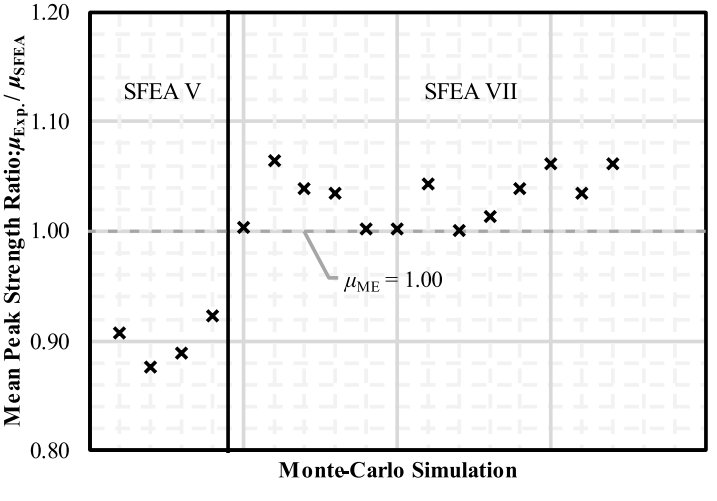

Figure 24. Distribution of the ratio between mean experimental and SFEA peak strength for diagonal tensile failure modes.

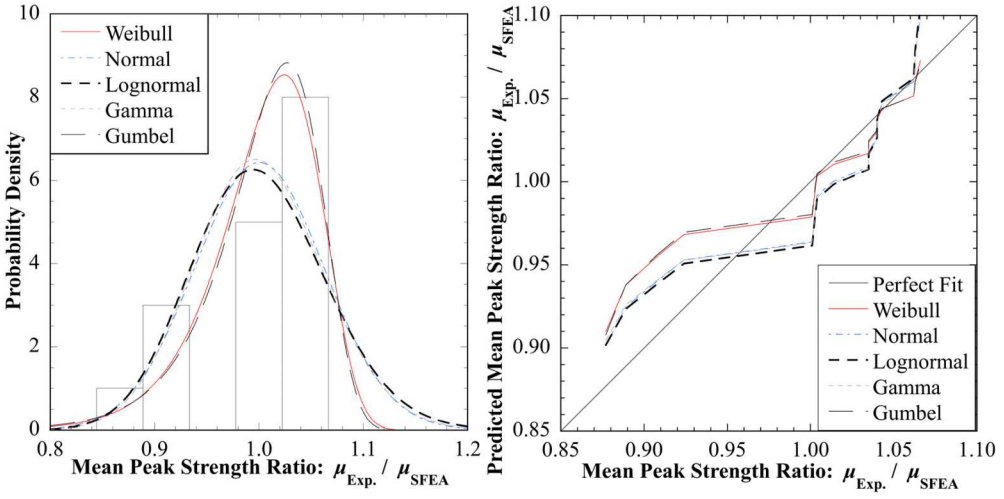

(a) PDFs of Mean Peak Strength Ratio: $\mu_{Exp.}$ / μ_{SFEA} (Diagonal Tension)

(b) CDF^{-1}s of Mean Peak Strength Ratio: $\mu_{Exp.}$ / μ_{SFEA} (Diagonal Tension)

Figure 25. Probabilistic distributions and inverse CDF plots of the ratio between mean experimental and SFEA peak strength for diagonal tension failures: (a) PDFs of mean peak strength ratio: $\mu_{Exp.}/\mu_{SFEA}$ (Diagonal Tension) and (b) CDF^{-1}s of mean peak strength ratio: $\mu_{Exp.}/\mu_{SFEA}$ (Diagonal Tension).

probabilistic distribution to describe ME, have been determined. These results are summarised in Table 10.

4.2. Derivation of model error variability

As discussed previously, the variability of ME, $V_{ME,}$ is a function of V_{SFEA} (summarised in Table 10) and the variability of the experimentally observed peak strengths, $V_{Exp.}$, as presented in Equation (8). $V_{Exp.}$ in turn is derived as a function of the measured variability of experimental peak shear strengths, $V_{measured}$ (summarised in Table 9), as well as the variabilities in the testing procedure, V_{test}, and in the specimens relative to a control specimen, V_{spec}.

4.2.1. Determination of test and specimen variability

To estimate suitable values for V_{test} for each failure mechanism, the COVs of the applied pre-compressions and in-plane displacements were examined. From this data, values of V_{test} equal to 0.015 and 0.017 have been determined for the experimental Wall Sets 1 and 2, respectively. While similar instrumentation was adopted for Sets 3 and 4, the increased complexity introduced with the addition of the pantograph system for Sets 3

Table 10. Summary of μ_{ME}, V_{SFEA} and the probabilistic distributions adopted for ME.

Failure mode	Sample size	μ_{ME}	V_{SFEA}	Distribution
Flexural tension	30	1.13	0.017	Lognormal
Flexural compression	32	1.09	0.035	Lognormal
Shear sliding	38	0.94	0.100	Lognormal
Diagonal tension	17	1.00	0.062	Lognormal

Table 11. Summary of variabilities for URM shear wall failure mechanisms.

Failure mode	Sample size	$V_{measured}$	V_{test}	V_{spec}	$V_{Exp.}$	V_{SFEA}	V_{ME}
Flexural tension	4	0.029	0.015	0.010	0.023	0.017	0.015
Flexural Compression	4	0.020	0.017	0.010	0.003	0.035	–
Shear sliding	3	0.050	0.040	0.010	0.028	0.100	–
Diagonal tension	4	0.099	0.040	0.010	0.090	0.062	0.065

and 4, as well as the larger size of the wall specimens, is expected to have increased the value of V_{test}. Of particular relevance are the potential friction losses in the pins included in the utilised truss arrangements (refer to Gooch et al. (2024)). As such, a value of V_{test} for Sets 3 and 4 equal to 0.04, in line with the recommendations of Ellingwood et al., (1980) for reinforced concrete beams and columns, has been assumed.

To estimate a value of V_{spec}, the variability in specimen length, height and thickness was examined. The in-plane shear capacity of an URM wall is directly proportional to the thickness, and in most cases the height, of the wall. Furthermore, this capacity is proportional to the length or length-squared of the wall in the case of shear- and flexure-based failure modes, respectively (Magenes and Calvi 1997). As such, the variabilities of these geometric properties are highly relevant to the peak in-plane shear capacity and are thus a reasonable proxy from which V_{spec} may be estimated.

From direct measurements of the length of each wall specimen, the variability in specimen length was determined to be approximately 0.005 for all four wall sets. However, specimen height was not directly measured. To supplement this data, the variability in wall height and length was estimated by considering the variability in bed and perpend joint thickness (after Mojsilović and Stewart (2015)) and the mean and COV of the height and length of the utilised masonry units. This assessment produced COVs ranging from 0.006 to 0.009. This statistical analysis was performed assuming no correlation between adjacent perpend joints, nor between successive bed joint courses (Heffler et al. 2008). Similarly, thickness of the laboratory wall specimens maintained a COV equal to 0.007. As such, a value 0.010 has been adopted for V_{spec} for all experimental sets.

Applying Equation (9), values for $V_{Exp.}$ were determined as presented in Table 11. Furthermore, applying Equation (8) to the derived values of $V_{Exp.}$ and V_{SFEA} (refer to Table 10) produces the values of V_{ME} shown in Table 11. Note that in the cases of a flexural compression or shear sliding failure a value of V_{SFEA} greater than the experimentally observed variability, $V_{Exp.}$ was determined, and thus the application of Equation (8) does not produce a value of V_{ME}. In such cases, a value of $V_{ME} = 0$ has been assumed (i.e. a deterministic value of ME). This result is not inconsistent with other, similar statistical analyses of URM structures. Isfeld et al. (2021) reports COVs for the ME of out-of-plane flexural failures ranging from 0 to 0.14 for walls of a similar geometry to those presented in this study. Similarly, Muhit (2021) reports values of V_{ME}, for an SFEA equal to 0 for the inward out-of-plane pressure loading and 0.06 for the outward out-of-plane pressure loading of URM veneer systems.

5. Conclusion

Seven spatially variable, stochastic finite element analyses (SFEAs) were performed on structural configurations consistent with the laboratory investigation presented by

Table 12. Summary of probabilistic models of ME.

Failure mode	Sample size	Mean	COV	Distribution
Flexural tension	30	1.12	0.02	Lognormal
Flexural compression	32	1.09	0	*Deterministic*
Shear sliding	38	0.94	0	*Deterministic*
Diagonal tension	17	1.00	0.07	Lognormal

Gooch et al. (2024). Models predicting either flexural tension or flexural compression failures produced accurate representations of the experimental specimens, with mean values of model error (ME) equal to 1.12 and 1.09, respectively. Furthermore, low variabilities in these MEs were determined, with a COV equal to 0.02 for flexural tension, and a COV of 0, indicating that a deterministic ME may be suitable, for a flexural compression failure. Conversely, SFEAs of shear sliding and diagonal tension failures produced poor representations of the experimental results. While the statistics of ME are similar to those for flexure, with mean values of 0.94 and 1.00, and COVs of 0 and 0.07 for shear sliding and diagonal tension, respectively, the load–displacement response of these numerical models were notably different to the experimental observations. In each case, the initial elastic stiffness was significantly overestimated, and the bilinear stiffness, such as is discussed by Al-Ahdal et al., (2022) and Medeiros et al., (2022) was not captured by the SFEAs. As such, predictions of shear behaviour made using the examined modelling methodology should be treated with caution, particularly where the limitations noted above are evident.

Despite these limitations, each SFEA produced reasonably accurate predictions of the peak in-plane shear capacities observed experimentally. Further applications of this modelling method, such as a reliability analysis of URM shear walls subject to the examined failure mechanisms may also consider the probabilistic models of ME presented in Table 12. In each case, a Lognormal distribution for ME was found to most accurately represent the data observed in this study. This result is consistent with the literature (JCSS 2002; Scholten et al. 2004), as well as previous, similar numerical investigations of URM structures (Isfeld et al. 2021; Muhit 2021).

A further limitation to the modelling technique presented in this paper is the computational expense associated with each Monte-Carlo simulation. The walls examined in this study were a half-storey in height and were subjected to a simplified quasi-static cyclic loading, rather than the dynamic loads imposed by seismic and wind events. Despite a simplified micro-model being adopted, each Monte-Carlo realisation took between several hours and several days to complete. As such, this technique may not be suitable to applications such as reliability analyses due to the requirement for a high accuracy in the estimation of the extreme lower-bound strength of a structure, an attribute that typically requires a large number of Monte-Carlo realisations. However, further refinement or simplification of the modelling method or an improvement in processing power may mitigate this limitation. Further research into the prediction of shear-base failure mechanisms is on-going.

Acknowledgements

The support of the Australian Research Council under Discovery Project DP220102758 is gratefully acknowledged.

Disclosure statement

No potential conflict of interest was reported by the author(s).

References

Al-Ahdal, A., N. Aly, and K. Galal. 2022. "Simplified Analytical Models for Partially Grouted Reinforced Masonry Shear Walls." *Engineering Structures* 252:113643. https://doi.org/10.1016/j.engstruct.2021.113643.

ASTM International. 2011. *Standard Test Methods for Cyclic (Reversed) Load Test for Shear Resistance of Vertical Elements of the Lateral Force Resisting Systems for Buildings*. West Conshohocken: ASTM International.

British Standards Institution. 2005. *BS EN1996-1-1: Eurocode 6: Design of masonry structures – Part 1-1: General Rules for Reinforced and Unreinforced Masonry Structures*. London: British Standards Institution.

Canadian Standards Association. 2014. *CSA S304-14: Design of Masonry Structures*. Mississauga: Canadian Standards Association.

CEN. 2002. *EN1052-3: Methods of Test for Masonry. Part 3: Determination of Initial Shear Strength*. Brussels: European Committee for Standardization.

Comite Euro-International Du Beton. 1991. *CEB-FIP Model code 1990. 203-205 ed*. Lausanne: Bulletines d'Information.

Corrêa, M. R. S., M. J. Masia, M. G. Stewart, and L. M. Heffler. 2012. "An Experimental and Statistical Analysis of the Flexural Bond Strength of Masonry Walls." *Australian Journal of Structural Engineering* 13: 139–148.

DIANA FEA. 2019. *DIANA 10.3 – User's Manual*. Delft: DIANA FEA.

Ellingwood, B., T. V. Galambos, J. G. MacGregor, and C. A. Cornell. 1980. *Development of a Probability Based Load Criterion for American National Standard A58. Special Publication 577 ed*. Washington, DC: National Bureau of Standards.

Farjada, S., and N. G. Shrive. 2023. "Statistical Analysis of Mortar Joint Thickness in Masonry Walls." In *Proceedings of the 14th North American Masonry Conference, Omaha*. Canada Masonry Design Centre.

Gooch, L. J., M. J. Masia, M. G. Stewart, and M. A. Hossain. 2024. "Experimental Testing of Unreinforced Masonry Shear Walls and Comparison with Nominal Capacity Predictions." *Journal of Structural Engineering*. In Press.

Gooch, L. J., M. J. Masia, M. G. Stewart, and C. Y. Lam. 2023. "Statistical Assessment of Tensile and Shear Properties of Unreinforced Clay Brick Masonry." *Construction and Building Materials* 386:131578. https://doi.org/10.1016/j.conbuildmat.2023.131578.

Hart, C. G., C. S. Huang, and A. T. Sabol. 1983. "Calibration of Strength Reduction Factors for Concrete Masonry." *Civil Engineering Systems* 1 (1): 33–36. https://doi.org/10.1080/02630258308970313.

Heffler, L. M. 2009. *Variability of Unit Flexural Bond Strength and its Effect on Strength in Clay Brick Unreinforced Masonry Walls Subject to Vertical Bending*. Callaghan: University of Newcastle.

Heffler, L. M., M. G. Stewart, M. J. Masia, and M. R. S. Correa. 2008. "Statistical Analysis and Spatial Correlation of Flexural Bond Strength for Masonry." *Masonry International* 21 (2): 59–70.

Howlader, M. K., M. J. Masia, and M. C. Griffith. 2020. "Numerical Analysis and Parametric Study of Unreinforced Masonry Walls with Arch Openings Under Lateral In-plane Loading." *Engineering Structures* 208:110337. https://doi.org/10.1016/j.engstruct.2020.110337.

Isfeld, A. C., M. G. Stewart, and M. J. Masia. 2021. "Stochastic Finite Element Model Assessing Length Effect for Unreinforced Masonry Walls Subjected to One-way Vertical Bending Under Out-of-plane Loading." *Engineering Structures* 236:112115. https://doi.org/10.1016/j.engstruct.2021.112115.

Isfeld, A. C., M. G. Stewart, and M. J. Masia. 2023. "Structural Reliability and Partial Safety Factor Assessment of Unreinforced Masonry in Vertical Bending." *Australian Journal of Structural Engineering* 24 (3): 191–205. https://doi.org/10.1080/13287982.2023.2173868.

JCSS. 2002. *Probabilistic Model Code. JCSS-OSTL/DIA/VROU-10-11-2000 - Part 3: Material Properties*. Joint Committe on Structural Safety. www. jcss-lc.org.

Konthesingha, K. M. C. 2012. *Earthquake Protection of Masonry Shear Walls Using Fibre Reinforced Polymer Strengthening*. Callaghan: University of Newcastle.

Lawrence, S. J. 1983. *Behaviour of Brick Masonry Walls Under Lateral Loading*. Sydney: University of New South Wales.

Lawrence, S. J., and H. T. Cao. 1988. "Cracking of Non-loadbearing Masonry Walls Under Lateral Forces." In *Proceedings of the 8th International Brick and Block Masonry Conference, Dublin*.

Lawrence, S. J., and J. P. Lu. 1991. "Cracking of Brickwork Walls with Lateral Loading." In *Proceedings of the Asia-Pacific Masonry Conference, Singapore*.

Li, J. 2015. *Spatial Variability and Stochastic Strength Prediction of Unreinforced Masonry Walls Subjected to Out-of-Plane Bending*. Callaghan: The University of Newcastle, Australia.

Li, J., M. G. Stewart, M. J. Masia, and S. J. Lawrence. 2016. "Spatial Correlation of Material Properties and Structural Strength of Masonry in Horizontal Bending." *Journal of Structural Engineering* 142 (11). https://doi.org/10.1061/(ASCE)ST.1943-541X.0001488.

Lourenço, P. B. 1996a. *A User/Programmer Guide for the Micro-modelling of Masonry Structures*. Delft: Delft University of Technology.

Lourenço, P. B. 1996b. *Computational Strategies for Masonry Structures*. Delft: Delft University of Technology.

Lourenço, P. B. 2008. "Structural Masonry Analysis: Recent Developments and Prospects." In *Proceedings of the 14th International Brick and Block Masonry Conference, Sydney*, 17–20. The University of Newcastle.

Lourenço, P. B., J. C. Almeida, and J. A. Barros. 2005. "Experimental Investigation of Bricks Under Uniaxial Tensile Testing." *Masonry International* 18 (1): 11–20.

Magenes, G., and G. M. Calvi. 1997. "In-plane Seismic Response of Brick Masonry Walls." *Earthquake Engineering & Structural Dynamics* 26 (11): 1091–1112. https://doi.org/10.1002/(SICI)1096-9845(199711)26:11<1091::AID-EQE693>3.0.CO;2-6

Magenes, G., P. Morandi, and A. Penna. 2008. *Test Results on the Behaviour of Masonry Under Static Cyclic in Plane Lateral Loads*. Pavia: Department of Structural Mechanics, University of Pavia.

Masia, M. J., et al. 2007. "Torsion Shear Test for Mortar Joints in Masonry: Preliminary Experimental Results." In *Proceedings of the 10th North American Masonry Conference, St. Louis*, 968–979. The Masonry Society.

The Masonry Society. 2022. *TMS 402/602-22 Building Code Requirements and Specification for Masonry Structures*. Colorado: The Masonry Society.

Mcneilly, T., J. Scrivener, S. J. Lawrence, and S. Zsembery. 1996. "A Site Survey of Masonry Bond Strength." *Australian Civil/Structural Engineering Transactions* 38: 103–109.

Medeiros, K. A. S., et al. 2022. "In-plane Behaviour and Seismic Performance of Differently Detailed, Multi-story, Perforated, Partially Grouted Masonry Walls." *Engineering Structures* 271. https://doi.org/10.1016/j.engstruct.2022.114941.

Melchers, R. E. 2007. "Structural Reliability Theory in the Context of Structural Safety." *Civil Engineering and Environmental Systems* 24 (1): 55–69. https://doi.org/10.1080/10286600601025191.

Melchers, R. E., and A. T. Beck. 2018. *Structural Reliability Analysis and Prediction. 3rd ed*. Hoboken: John Wiley & Sons Ltd.

Mojsilović, N., and M. G. Stewart. 2015. "Probability and Structural Reliability Assessment of Mortar Joint Thickness in Load-Bearing Masonry Walls." *Structural Safety* 52:209–218. https://doi.org/10.1016/j.strusafe.2014.02.005.

Muhit, I. B. 2021. *Stochastic Assessment of Unreinforced Masonry Veneer Wall Systems Subjected to Lateral Out-of-Plane Loading*. Callaghan: The University of Newcastle.

NZSEE. 2017. *The Seismic Assessment of Existing Buildings*. Wellington: New Zealand Society for Earthquake Engineering.

Petersen, R. B. 2009. *In-plane Shear Behaviour of Unreinforced Masonry Panels Strengthened with Fibre Reinforced Polymer Strips*. Callaghan: The University of Newcastle, Australia.

Petersen, R. B., M. J. Masia, and R. Seracino. 2008. "Experimental Verification of the Finite Element Model to Predict the Shear Behaviour of NSW FRP Strengthened Masonry Walls." In *Proceedings of the 14th International Brick and Block Masonry Conference, Sydney*. The University of Newcastle.

Rots, J. G. 1997. *Structural Masonry: An Experimental/Numerical Basis for Practical Design Rules*. Rotterdam: A.A. Balkema.
Scholten, C. v., et al. 2004. *Reliability-Based Classification of the Load Carrying Capacity of Existing Bridges: Report 291*. Copenhagen: Road Directorate.
Standards Australia. 1998. *AS4100: Steel structures*. Sydney: Standards Australia.
Standards Australia. 2018. *AS 3700: Masonry structures*. Sydney: Standards Australia.
Stewart, M. G., and S. J. Lawrence. 2007. "Model Error, Structural Reliability and Partial Safety Factors for Structural Masonry in Compression." *Masonry International* 20 (3): 107–116.
Tomaževič, M. 1999. *Earthquake-Resistant Design of Masonry Buildings*. London: Imperial College Press.
Van der Pluijm, R. 1997. "Non-linear Behaviour of Masonry Under Tension." *Heron* 42 (1): 25–54.